Pressure Fields and Fluid Acceleration

Ascher H. Shapiro
MASSACHUSETTS INSTITUTE OF TECHNOLOGY

Fluid dynamics deals with the motions of gases and liquids and with how these motions are related to forces. For this film, we have designed *steady-flow* experiments in which all body forces (gravitational, electromagnetic, etc.) as well as viscous forces, are relatively unimportant, and in which the fluids are essentially *incompressible*. The main force accounting for the fluid acceleration is the pressure gradient.

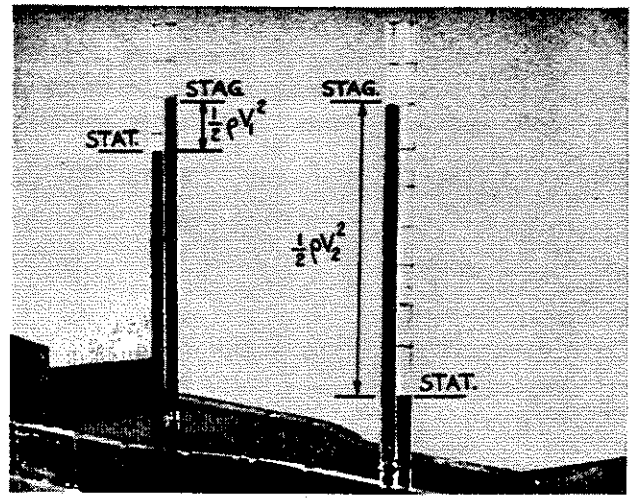

1. Water flows from left to right. The manometer tubes marked "STAT"are connected to static pressure taps at the upstream and downstream cross-sections. Those marked "STAG" are connected to upstream-facing pitot tubes.

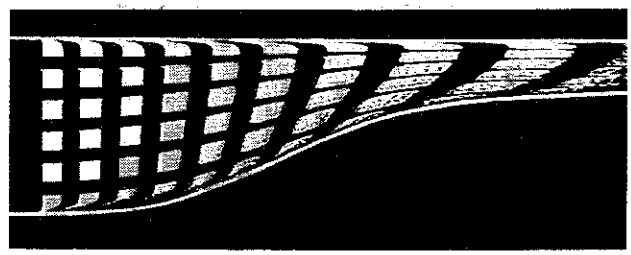

2. Water flows from left to right. Tiny hydrogen bubbles are electrolyzed at a wire near the entrance. Segments of the wire are insulated, and the current is pulsed. Thus square patches of bubbles are released.

Pressure Variation Along Streamlines

Our first experiments have to do with changes of pressure and velocity in the streamwise direction. Fig. 1 shows water flowing through a channel of decreasing cross-sectional area. The static-pressure manometers indicate that the pressure decreases in the direction of flow.

Since water is nearly incompressible, the volume flow entering the contraction must equal the volume flow leaving. But the volume flow Q is equal to AV, where V is the average velocity and A is the cross-sectional area; hence the area decrease should produce a velocity increase. The velocity field is shown in Fig. 2. Each fluid patch accelerates as it goes

through the contraction. Because of the longitudinal velocity gradient, the front edge of each patch moves faster than the rear edge; hence each patch stretches out. Since water is virtually incompressible, and the flow is two-dimensional, the area of each patch cannot change; thus each becomes narrower as well as longer. The successive bubble patches mark out the streaklines of the flow and, (since the motion is steady) the streamlines as well.

The velocity increase inferred from Fig. 2 is related to the pressure decrease of Fig. 1 by Newton's law of motion. For some kinds of analysis, it is convenient to use distance along the streamlines, s, and distance along the normal trajectories to the streamlines, n, as curvilinear coordinates. Since viscous stresses are negligible, the normal stress at a point is the same in all directions. It is the scalar hydrostatic pressure, p. The net force acting along s, arising from the pressure gradient $\delta p/\delta s$, is related to the fluid acceleration along s by Euler's equation of steady inviscid motion along the streamline:

$$\delta p/\delta s = -\rho V(\delta V/\delta s) \qquad \text{(Eq. 1)}$$

The minus sign tells us that a velocity *decrease* in the streamwise direction is accompanied by a pressure *increase*, and vice versa.

Fig. 3 shows flow through a manifold, with bleed valves installed to allow withdrawal of fluid at several stations between the manometer tubes. With the bleed valves closed, the average water velocity is the same at all cross-sections, and there is a barely perceptible pressure drop due to viscous forces. The volume flow is then reduced in each successive cross-section by bleeding water away through the valves. The pressure now *rises*. Since the area A is in this case constant, the velocity V is proportional to the volume flow Q; hence the velocity V decreases along s, and $\delta V/\delta s$ is negative. In agreement with Eq. 1, $\delta p/\delta s$ is positive.

In an incompressible, steady, inviscid flow, Euler's equation may be integrated with respect to distance along each streamline, to obtain the Bernoulli integral,

$$p + \rho V^2/2 = \text{constant} = p_{\text{stag}} \qquad \text{(Eq. 2)}$$

Along each streamline the sum of the static pressure p and the dynamic pressure $\rho V^2/2$ is a constant. This sum is called the *stagnation pressure*, or *total pressure*. On any one streamline, wherever the velocity is high, the pressure is low, and vice versa. The highest possible pressure, the stagnation pressure, occurs where the velocity is zero. A large reservoir supplying a fluid to a duct system is itself a stagnation region.

Fig. 4 shows a streaming flow past a blunt-nosed body, with a central stream tube marked by hydrogen bubbles. The widening of this stream tube shows that the flow is decelerating. Where the central streamline reaches the nose is a stagnation point. There the speed is zero. On both sides of the unique stagnation streamline the fluid decelerates, although not to zero speed, and then accelerates as it slides around the sides.

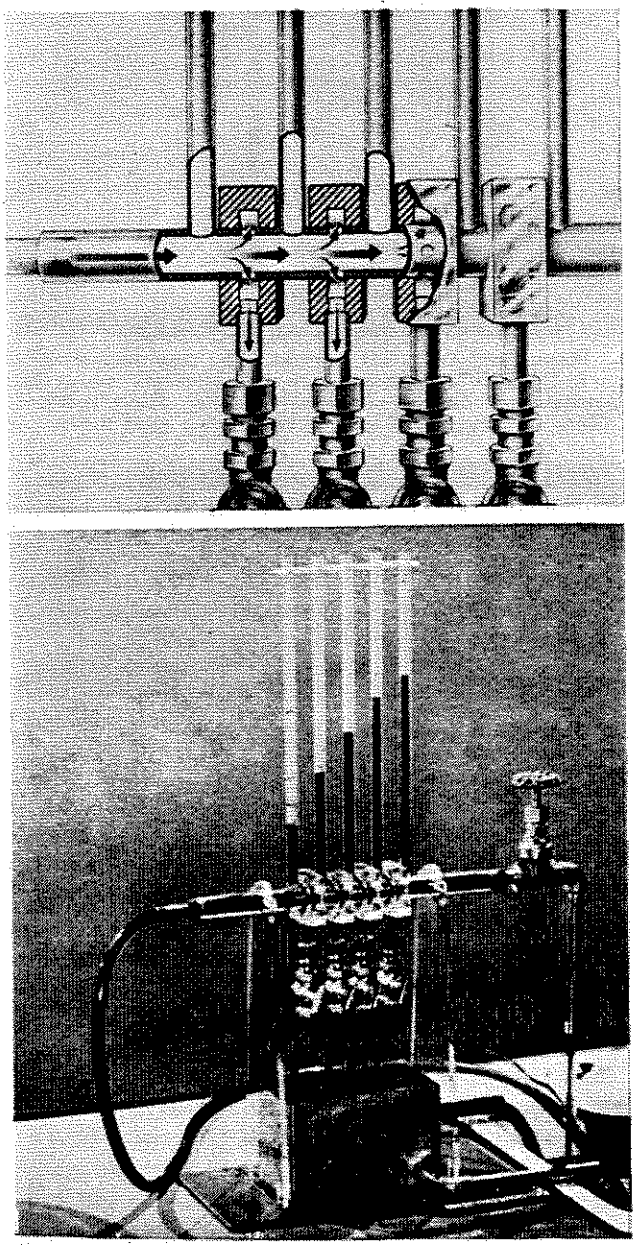

3. Water flows through a manifold from left to right. Five manometer tubes, open at the top, show the longitudinal pressure distribution when fluid is withdrawn through the open bleed valves.

4.

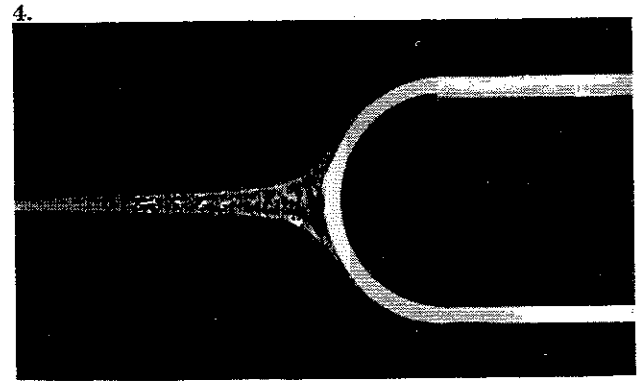

The experimental realization of a stagnation point is put to practical use in a pitot tube. The hole at the upstream-facing nose measures the stagnation pressure of the particular streamline reaching the hole, as defined by Eq. 2. In the contracting flow of Fig. 1, pitot tubes at the upstream and downstream cross-sections of the contraction show the respective stagnation pressures. By Eq. 2, the difference between the local stagnation pressure and the local static pressure is the local dynamic pressure. Thus (Fig. 1), we may determine the fluid speed through a measurement of this difference. Furthermore, Fig. 1 verifies that although both the dynamic pressure and the static pressure vary in the contraction, the sum of the two — the stagnation pressure — remains constant.

Bernoulli's integral also explains how suction can be produced by blowing, as in the aspirator experiment of Fig. 5. To illustrate in detail how a venturi can produce low pressure, Fig. 6 shows an experiment with flow through an unsymmetrical venturi in which one wall is straight. Since AV is constant, the average cross-sectional velocity increases to the throat; in accord with Eq. 1, the pressure decreases. Downstream of the throat, the area increase produces a velocity decrease, and the pressure rises. At the upstream and downstream ends, where the cross-sectional areas are equal, the average velocities are also equal. Bernoulli's integral predicts equal pressures, but the downstream pressure is substantially less than the upstream pressure. The static-pressure recovery in the diffuser is only about half of the static-pressure decrease to the throat. This difference is due to viscous boundary layers whose behavior we must always keep in mind

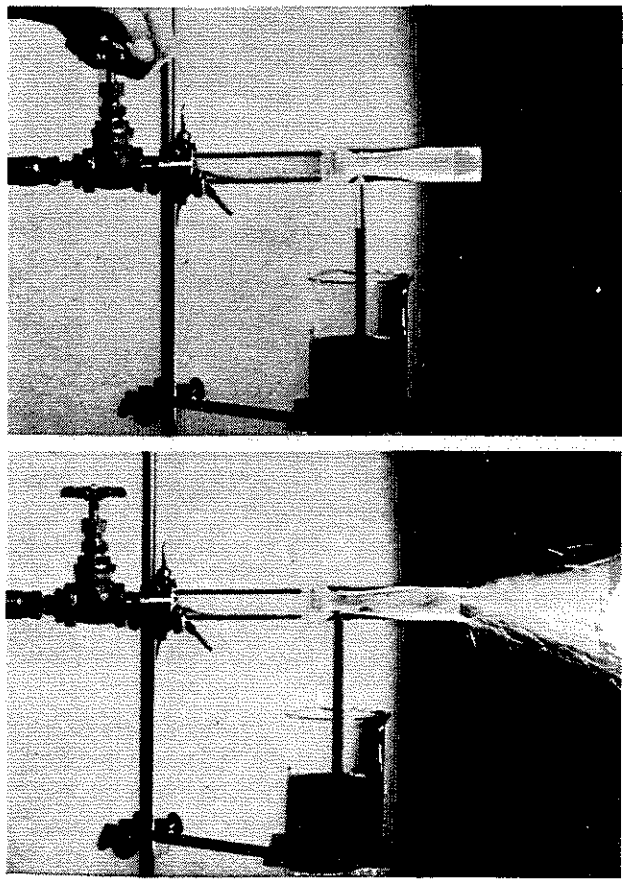

5. Air is blown from left to right through a venturi. The sub-atmospheric pressure at the throat sucks up water from a beaker.

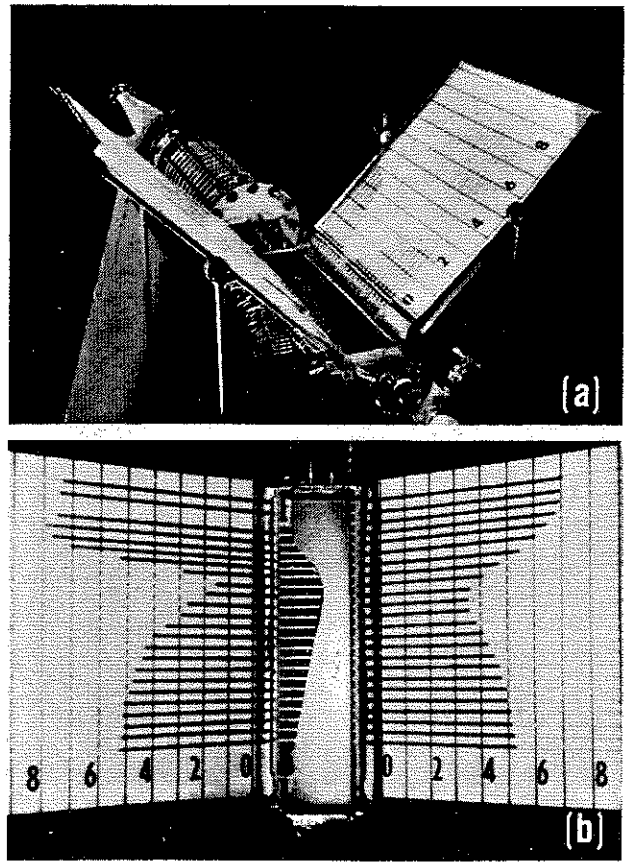

6. (a) A two-dimensional horizontal venturi-tube test section is installed at the exit of the large settling section. Pressure leads from each wall of the channel are connected to the two manometer boards inclined at 45°. (b) Overhead view of pressure distribution on the straight and curved walls of the venturi. Water flow is from top to bottom.

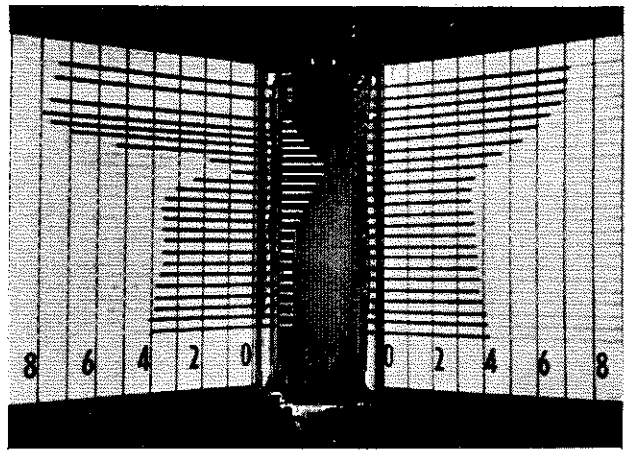

7. Pressure distributions for a venturi in which the diffuser diverges so rapidly that flow separation occurs and there is little pressure recovery. Compare with Fig. 6b.

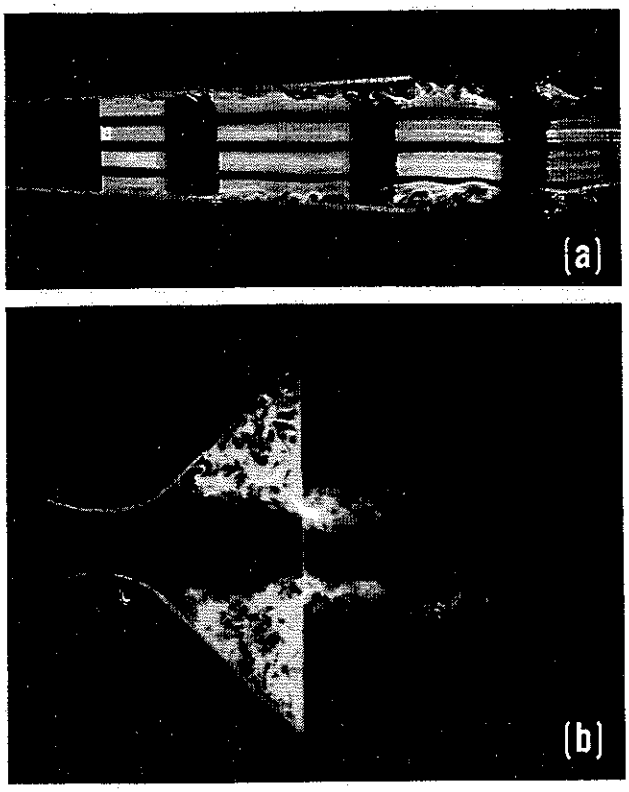

8. Hydrogen bubbles mark the flow in a diffuser. Flow is from left to right. (a) Small divergence angle. The flow remains attached. (b) Large divergence angle. The flow detaches.

even when we pretend temporarily that viscosity is absent. In the experiment of Fig. 7, the area divergence is too rapid, and the static pressure recovery in the diffuser is only about a quarter of the decrease in static pressure to the throat. Even a very small amount of viscosity, if it leads to boundary-layer separation (Fig. 8), can produce radical changes from a hypothetical non-viscous flow.

In the experiment of Fig. 9, water flows through a venturi that discharges to the atmosphere. Since the pressure at the exit is atmospheric, the throat pressure is sub-atmospheric. As we increase the flow, all pressure differences increase with the square of the velocity. When the absolute pressure at the throat goes below the vapor pressure of water (about one inch of mercury), boiling occurs. This is cavitation. Steam bubbles appear in the water. Their subsequent collapse creates enormous pressures which can be clearly heard as sound and which can produce very high stresses on nearby walls. Such mechanical stresses often do great damage to liquid-handling machinery, to marine hydrofoils and propellers, and to hydraulic structures.

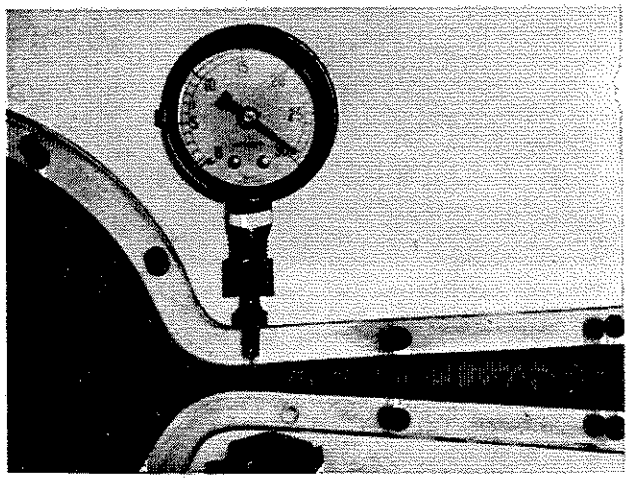

9. Flow of water, from left to right, through a venturi which discharges to the atmosphere. The gauge shows the vacuum at the throat, in inches of Hg. below atmospheric. When the vacuum reaches nearly 30″ Hg., cavitation zones appear near the throat. These are seen in the photo as dark patches.

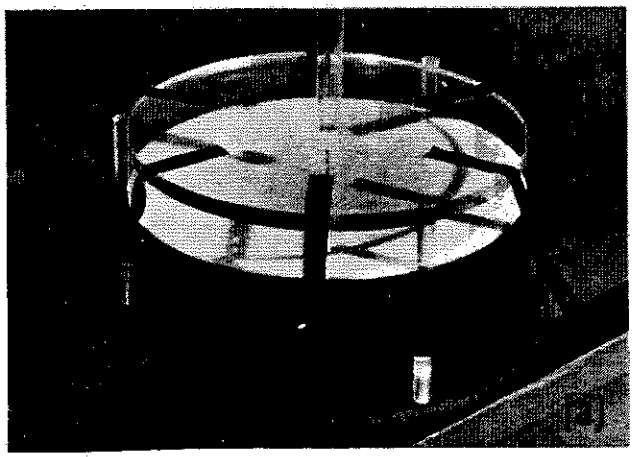

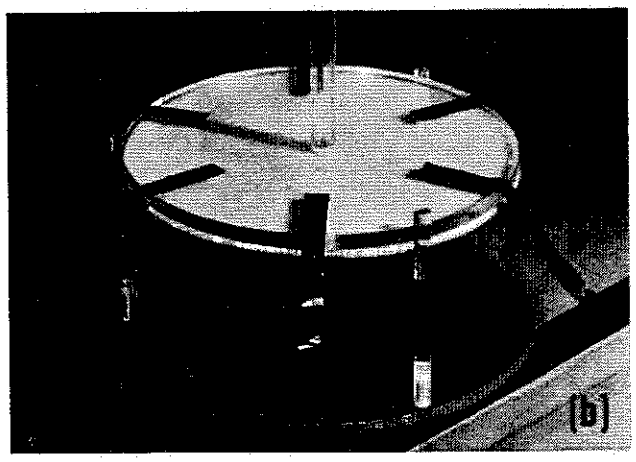

10. The white plastic disk is free to move vertically. The thick clear disk at top is supported from the base on three posts. Air blown down through the vertical tube at the top escapes rapidly in the space between the white disk and the clear disk. The black streamers indicate the escaping air flow. (a) No air flow. The streamers are limp, and the white disk rests on stops. (b) The air flow is on, and the streamers are extended. The white disk is lifted upward by the downward air flow, until only a small gap separates it from the clear disk.

When air is blown from a hole in the middle of one disk against a parallel disk (Fig. 10), the resulting pressure distribution can be such as to force the disks together. To see how this happens, we have instrumented the lower plate (Fig. 11a) with pressure taps attached to manometer tubes below. Note that the water in each manometer tube is pushed down when the pressure goes above atmospheric. At the disk axis,

the pressure is greater than atmospheric by an amount equal to the dynamic pressure of the air jet. Over most of the plate, though, the pressure is less than atmospheric, and rises to atmospheric pressure at the outer edge. The reason is that the through-flow cross-sectional area between the disks increases with radius. This area increase causes a fluid deceleration and, by Bernoulli's integral, a pressure rise to the atmospheric pressure at the outer edge. The sub-atmospheric pressure over most of the area accounts for the disks being forced together. Actually the viscous forces are by no means negligible. For the equilibrium position, however, the inertial forces are generally larger than the viscous forces and govern the shape of the pressure distribution.

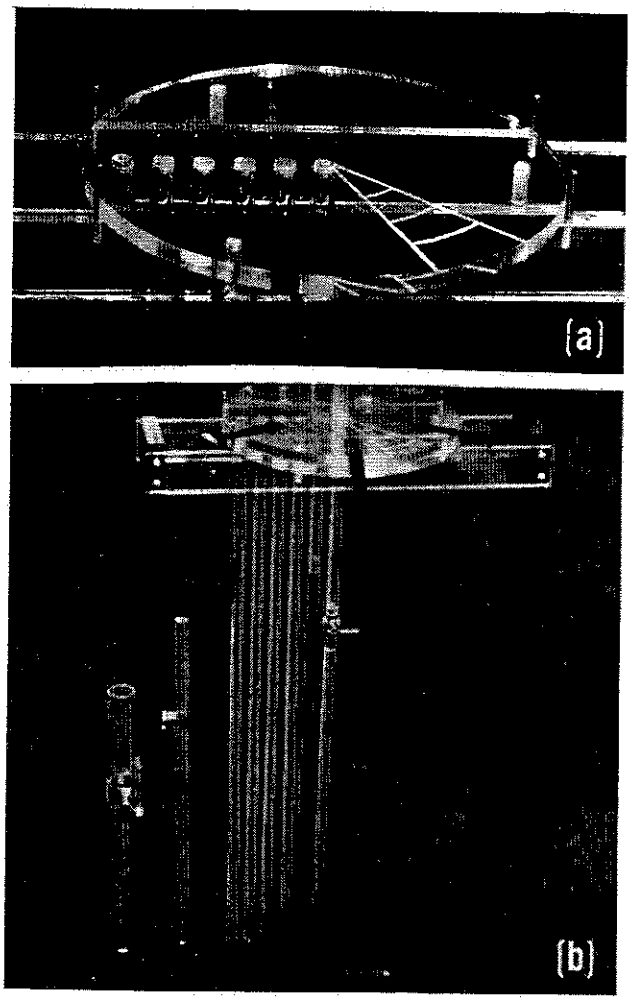

11. (a) A fixed lower disk for the experiment of Fig. 10, with six static pressure taps and manometer tubes attached below. Three small gap spacers are visible, on which the upper disk of Fig. 10 is placed. (b) The six manometer tubes are connected through a common header (out of frame at bottom) to the large reservoir at the far left. The single manometer tube at the left is open at the top and indicates atmospheric pressure. The manometers show the pressure in the gap is below atmospheric except near the axis of the air jet. There the pressure is so high that the liquid level is out of sight.

Pressure Variation Normal to Streamlines

Thus far we have discussed the relationship between pressure changes and velocity changes *along* a streamline, or on the average along a channel. However, Fig. 7 shows how different the pressure distributions may be along the two walls of an unsymmetrical channel. To understand this, we must consider the particle dynamics in a direction normal to the streamline.

Let R be the local radius of streamline curvature. The pressure gradient $\delta p/\delta n$, acting on the fluid particle toward the center of curvature is related to the acceleration V^2/R by Euler's equation of inviscid motion normal to the streamline,

$$\delta p/\delta n = \rho V^2/R \qquad \text{(Eq. 3)}$$

which shows that the pressure always increases outward from the center of curvature.

The channel bend of Fig. 12 produces curved streamlines. In the straight section approaching the bend the streamlines are nearly straight and the pressure gradient normal to the streamlines is virtually zero. The difference between the entering stagnation pressure and the static pressure at the upstream tubes is a dynamic pressure of about eleven inches of water. At the middle of the bend, where streamline curvature is pronounced, there is a pressure difference between the two sides of the channel, normal to the streamlines, of about three and a half inches of water. Downstream of the bend the pressure is almost uniform again (the slight variation is due to a complicated secondary flow induced by the bend).

Returning to Fig. 6b, we see that the throat pressure

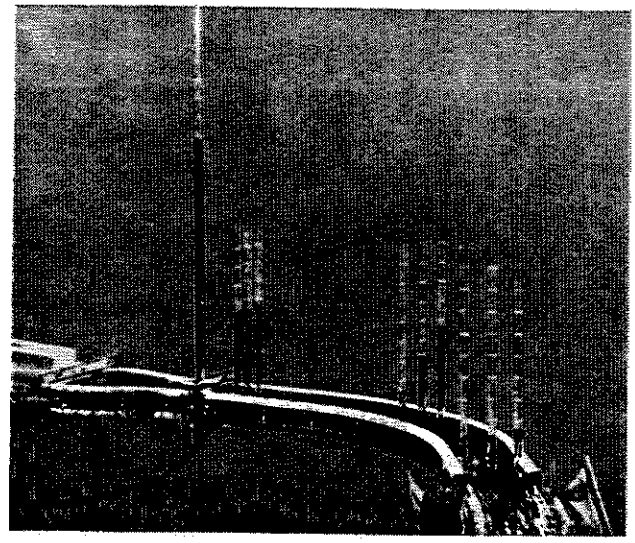

12. Flow in a two-dimensional 80° bend, entering from large settling chamber at left and discharging toward viewer at right. Each set of three static pressure manometers shows the transverse pressure distribution in a plane normal to the flow. The first and last sets are in straight sections of the channel, while the middle set is in the mid-point of the bend. The single manometer tube at left shows the stagnation pressure.

on the curved wall is considerably less than at the straight wall, with the pressure increasing in the direction away from the center of streamline curvature, as demanded by Eq. 3. When we use venturis for flow measurement, the pressure we measure at the wall is thus not the average pressure at the throat.

When you place your finger near the side of a jet from a water faucet, the jet bends toward your finger. This is the Coanda effect. In Fig. 13 the jet attaches to and bends around a freely-suspended hollow cylinder which has in it a small static pressure hole connected to a manometer. Since the streamlines are curved, there is a normal pressure gradient, with the pressure at the cylinder surface less than the atmospheric pressure at the outside boundary of the jet. Because of this sub-atmospheric pressure, the jet is bent around the cylinder, and there is a net force on the cylinder acting toward the jet.

The Coanda effect is also part of the explanation for the fact that a billiard ball may be supported by a rather small air jet (Fig. 14).

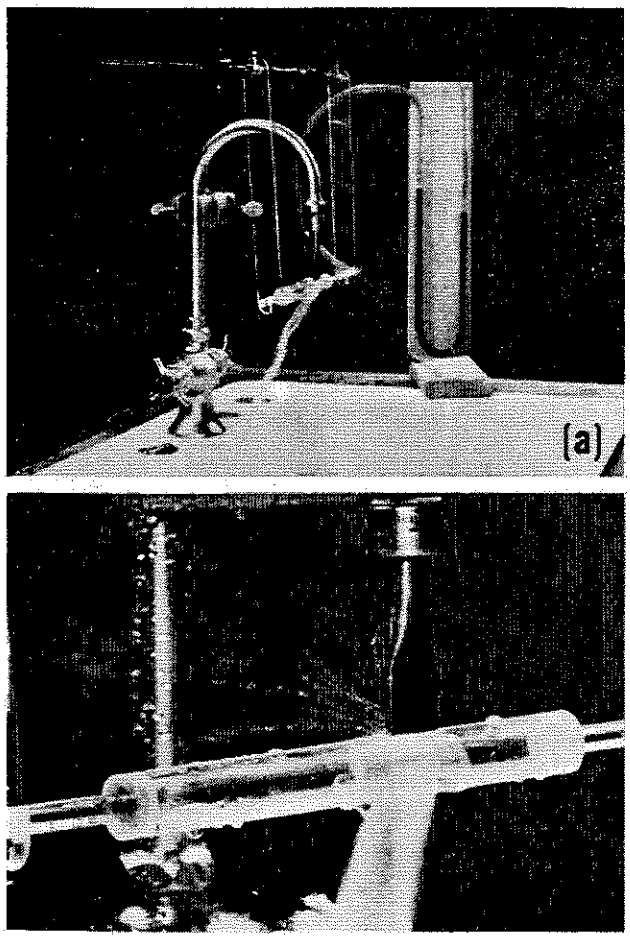

13. Jet of water from a slit nozzle. Behind and below it is a hollow closed cylinder hanging freely and vertically from pivots. When the cylinder is brought next to the jet, the latter attaches to and bends around the cylinder. The sub-atmospheric pressure on the cylinder surface is sensed at a pressure tap and transmitted to the manometer. The resulting pressure distribution on the cylinder produces on it a force directed toward the jet, as shown by the inclination of the pendulum support.

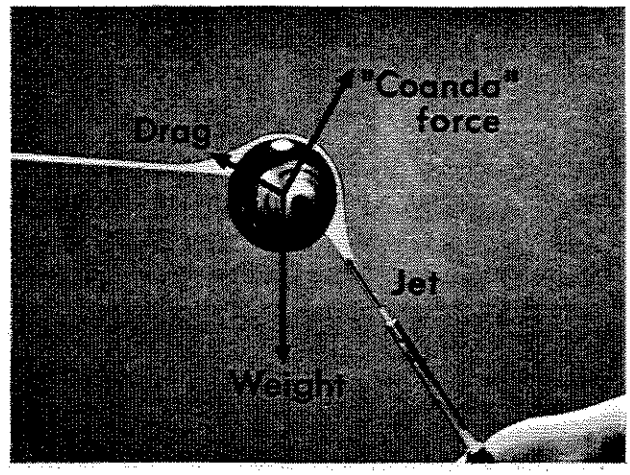

14. A billiard ball is supported by an air jet supplied by a ⅛" diameter nozzle at 60 psig. The superposed drawing shows the forces on the ball accounting for its equilibrium.

Complete Pressure Field

We have now looked separately at the pressure gradients along and normal to the streamlines. To understand a complete flow pattern, however, we must consider both gradients simultaneously, and we must also consider the equation of continuity.

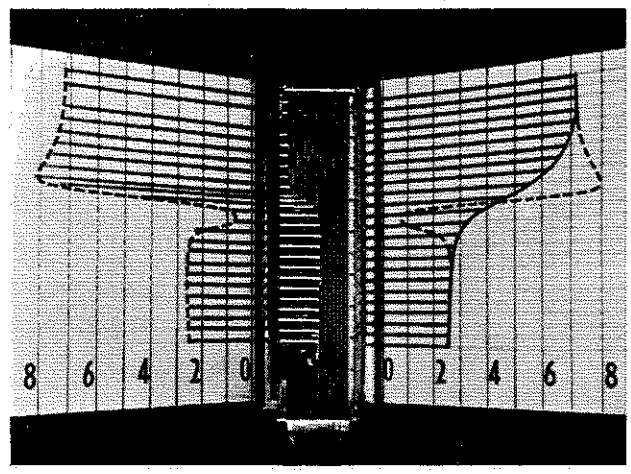

15. Wall pressure distributions for flow through a rapid unsymmetrical contraction. The dashed curve compares the distribution on the curved wall with that on the straight wall.

Fig. 15 compares the pressure distributions on the two walls of a rapid unsymmetrical contraction. Upstream, the pressures are equal on both walls. Downstream, they are also equal but lower. Because of the general area decrease, the average velocity increases. In agreement with Eq. 1, the average pressure falls.

On the straight wall the pressure falls continuously. But on the curved wall it first rises, then undershoots to a very low value, then rises once again to its final value.

These two pressure distributions may be interpreted using the two dynamical equations and the equation of continuity. The middle curve of pressure versus distance in Fig. 16 shows the streamwise variation of the

average pressure at each cross-section as determined (through Bernoulli's integral) by the average velocity at each cross-section. Far upstream and far downstream, where the streamlines have virtually no curvature, the pressure is uniform over the cross-sections.

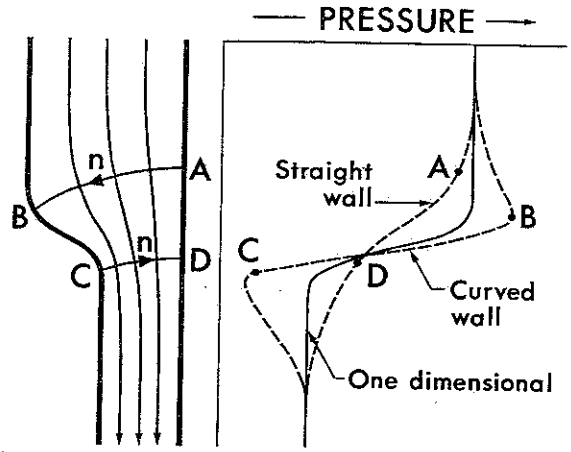

16.

From the shape of the channel, we may expect that the streamlines will be generally of the shape sketched in Fig. 16; concave to the right in the neighborhood of AB; concave to the left in the neighborhood of DC. The curves AB and DC are drawn normal to the streamlines in regions of different concavity. The arrows on these curves show the directions of increasing n. From one-dimensional considerations and a comparison of cross-sectional areas, the average pressure on AB is only slightly less than the upstream pressure. But, because of streamline curvature, the pressure increases from A to B. Hence the pressure at B is greater than the upstream pressure, and that at A is less. Similarly, the average pressure on CD is only slightly greater than the downstream pressure, but again, because of streamline curvature, the pressure increases from C to D. Hence the pressure at D is greater than the average, and that at C is less than the average. Putting all this together, we can understand why the pressure on the curved wall first rises to a maximum at B and then falls to a minimum at C, while on the straight wall it falls continuously from A to D.

According to Bernoulli's integral, which in this case has the same stagnation pressure for each streamline, the velocity is a minimum where the pressure is highest and a maximum where the pressure is least. The hydrogen bubble lines of Fig. 17 verify the velocity distributions which may be inferred from the pressure distributions of Figs. 15 and 16 by using Bernoulli's integral. The tilting of these fluid lines shows that, near the beginning of the contraction, the velocity near the curved wall is less than that near the straight wall.

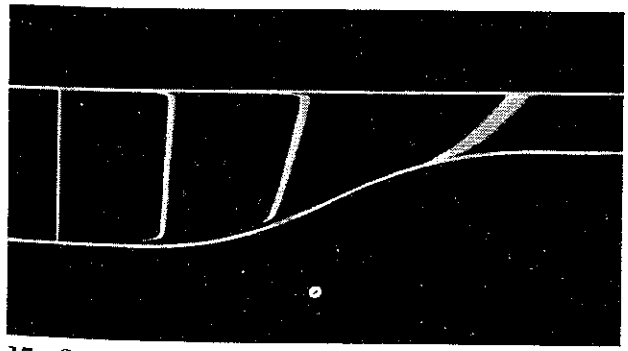

17. Successive positions of a bubble line which is initially vertical.

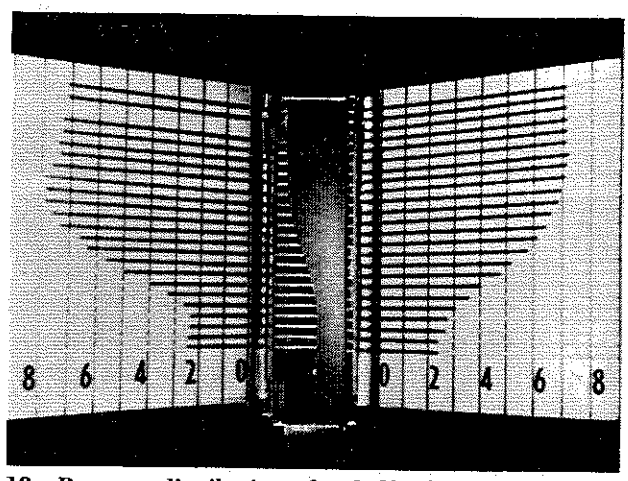

18. Pressure distributions for half of a gradual symmetrical contraction. Compare with Fig. 15.

To avoid separation of the flow from the walls due to adverse pressure gradients in wind tunnel nozzles, contractions are made gentle, as in Fig. 18. The streamline curvature here is much less than in Fig. 15, and the transverse pressure gradients which cause the distinctive peaks in the pressure distribution of Fig. 15 are reduced.

Bernoulli's Integral Is Not Always Valid

The statement "high velocity means low pressure" is only sometimes true. Viscosity or compressibility or unsteadiness can render Bernoulli's integral invalid, and the integral applies only to individual streamlines unless the motion is irrotational.

The straight duct of Fig. 19 has a partition. One side is free and clear; the other side has a flow resistance. The static pressures shown by the manometers are equal. However, to conclude from Bernoulli's integral that the velocities of the two streams are also equal would be wrong. The stagnation pressures of the two adjoining streams are actually quite different. From the two dynamic pressures we see that the velocity in the obstructed passage is less than that in the clear passage. The reason Bernoulli's integral cannot be used here to interpret the observed static pressures is that we are dealing with different streamlines having different stagnation pressures. We must instead use Eq. 3: because of the confinement of the channel walls, the streamlines have virtually no curvature; thus the normal pressure gradient is zero, and the

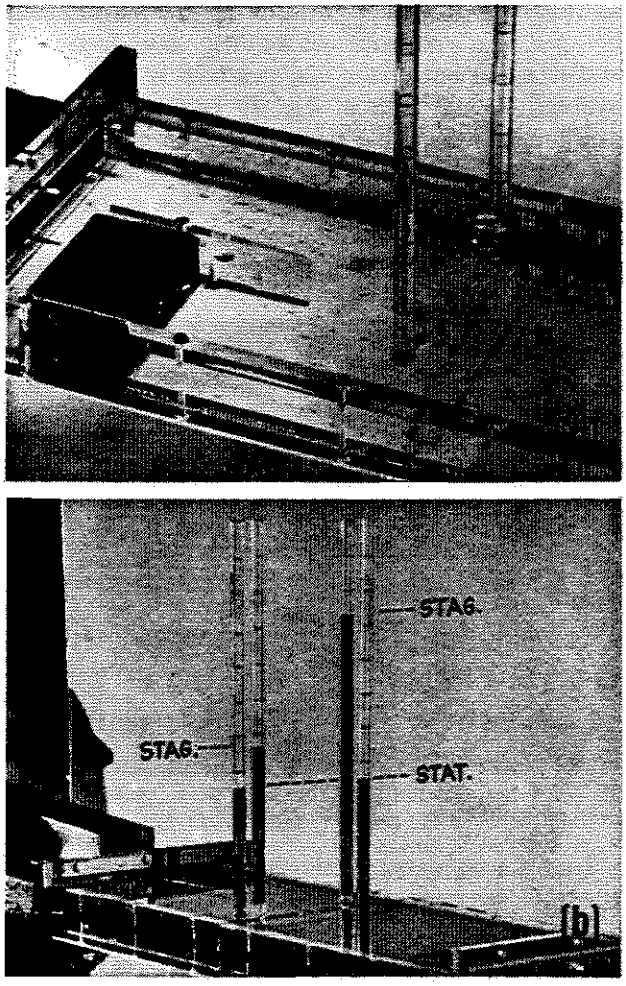

19. (a) A straight duct with a divider at the left. Both halves of the flow come from a common reservoir, but the lower half passes through a bank of small tubes which act as a flow resistance. Downstream of the partition the two halves of the flow are again in contact. (b) The flow is on. The two outer manometers show the static pressures, while the two inner manometers are connected to upstream-facing pitot tubes and show stagnation pressures.

static pressures in the two streams are the same even though the velocities differ. For the same reason, the static pressure across a viscous boundary layer is virtually constant.

The vertical tubes of Fig. 20 show the pressure distribution in a horizontal tank of water when we rotate it on a turntable. After viscosity forces the water into solid body rotation, the velocity increases linearly with radius, that is $V = \Omega r$. If we used Bernoulli's integral (which would be improper because we would be crossing streamlines), we might expect the pressure

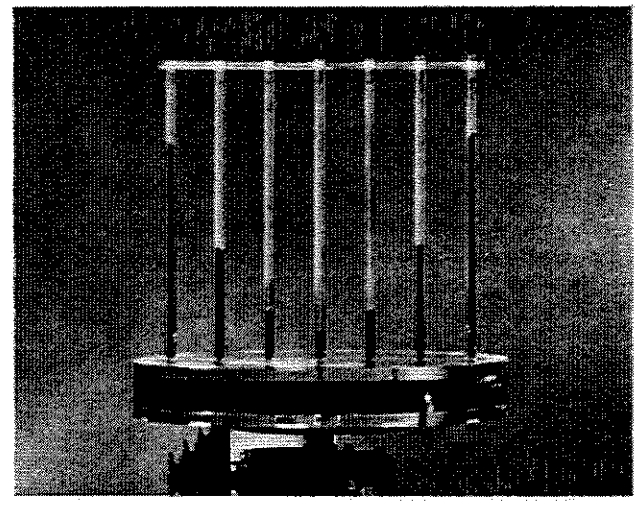

20. A closed cylindrical tank of colored water is mounted on a horizontal turntable. The manometer tubes mounted in the cover are open at the top to atmosphere, and show how the pressure varies with radius. With the tank initially at rest, the level is the same in all the tubes. After the turntable has rotated at uniform speed for a long time, the water is in solid-body rotation, locked by viscosity to the tank. This picture was taken at an instant when the rotating bank of manometer tubes was normal to the line of view.

to *decrease* with radius. Actually, the pressure *increases* with radius. This means that the stagnation pressure also increases with radius, and that each circular streamline has a different Bernoulli constant. The right way to look at this is with Equation 3:

$$\delta p/\delta n = \rho V^2/R = \rho\Omega^2 r^2/R$$

But, for circular motions, $\delta p/\delta n = dp/dr$, and $R = r$. Thus, $dp = \rho\Omega^2 r dr$, which integrates to $p = \rho\Omega^2 r^2/2 +$ constant. This is the parabolic pressure distribution of Fig. 20.

Reference

Prandtl, L.: *Essentials of Fluid Dynamics,* Chapter 11. Hafner Publishing Co., New York, 1952.